Development of a Darcy- Brinkman model to simulate water flow and tracer transport in a heterogeneous karstic aquifer (Val d'Orléans, France)

Ali Salim Joodi, Stanislas Sizaret, Stéphane Binet, Ary Bruand, Patrick Albéric, Michel Lepiller

Development of a Darcy- Brinkman model to simulate water flow and tracer transport in a heterogeneous karstic aquifer (Val d'Orléans, France)

Ali Salim Joodi [1*], Stanislas Sizaret [1], Stéphane Binet [1], Ary Bruand [1], Patrick Alberic [1], Michel Lepiller

Université d'Orléans, CNRS/INSU, Université de Tours, Institut des Sciences de la Terre d'Orléans (ISTO), UMR6113, 1A rue de la Férollerie 45071 Orléans, Cedex 2 France.

*** Corresponding author**

Université d'Orléans, CNRS/INSU,

Institut des Sciences de la Terre d'Orléans (ISTO)

Université d'Orléans – CNRS/INSU

1A rue de la Férollerie

45071 Orléans Cedex 2, France

E-mail: Ali.Joodi@univ-orleans.fr

Tel : 332 38 25 53 96

Fax : 332 38 63 64 88

Abstract Modelling karstic aquifers is problematic because the equation of references (i.e. Darcy) is adapted to describe hydrodynamics of flow in a rock where porosity is low. The modelling of the karstic drains requires to use a macroscopic equation representative of the physics of flows occurring in rock where pores are important in size. To answer this question, our study presents an example of the hydrodynamic model adapted to the karstic aquifer of the Val d'Orléans starting from two equations characterizing the dynamics of the fluids: i) the Darcy law used to describe the hydraulic behaviour of massive limestone, and ii) the equation of Brinkman models the flows in vacuums of big sizes within the karstic drain. In the second objective, the flow equations are coupled with the transport equation to predict the karst properties. The results are tested by using six tracer tests carried out in the Val d'Orléans. The simulations show that the draining permeability ranges from 5×10^{-6} to 5.5×10^{-5} m^2, the limestone permeability ranges from 8×10^{-11} to 6×10^{-10} $m^{2.}$ The dispersivity coefficients in the drains range from 23 to 43 m and in the fractured zone from 1 to 5 m.

Résumé La modélisation des aquifères karstiques est problématique car l'équation de Darcy, employée généralement pour décrire les écoulements, est adaptée pour les milieux où la porosité est faible. La modélisation des drains karstiques nécessite d'utiliser une loi macroscopique représentative de la physique des écoulements qui ont lieu dans les systèmes où les pores sont de taille importante. Pour répondre à cette question, notre étude présente un exemple de modèle hydrodynamique adapté aux aquifères karstiques du Val d'Orléans: i) La loi de Darcy employée pour modéliser le comportement hydraulique des calcaires massifs, et ii) l'équation de Brinkman décrivant les écoulements dans les vides de grandes tailles caractérisant les zones de drainage karstique. Ensuite, les équations des écoulements sont couplées avec l'équation de transport pour prédire les propriétés du karst. Les résultats sont calibrés en utilisant six essais de traçages réalisés dans le Val d'Orléans. Les simulations montrent que la perméabilité du drain s'étend de 5×10^{-6} to 5.5×10^{-5} m^2, la perméabilité des calcaires fracturés s'étend de 8×10^{-11} to 6×10^{-10} m^2. Les coefficients de dispersivité dans les drains s'étendent de 23 à 43 m et dans les calcaires fracturés de 1 à 5 m.

Keywords: Groundwater flow. Karst. Numerical modelling. Solute transport. Brinkman equation

Introduction

Karst aquifers are often considered as resulting from two interconnected flow systems that developed (i) in the fracture network of the limestone bedrock and (ii) in the conduit network that is specific of a karst system. The fractured limestone bedrock has a high storage capacity because of the low mobility of water located in the fissures and the presence of almost stagnant water in the porous matrix (Hauns et al. 2000). Most water enters the karst system at the catchment surface through swallow holes points and flows through the fractured aquifer to drainage channels, finally drained by karst springs. Thus, in karstified media all types of porosity are present, including porous and fine fissure porosity, large fissure porosity and karst channels.

In the past several decades, quantitative modeling of karst groundwater flow can be classified into three types of approach:

(1) The black-box approaches that ignores the complexity of flow regimes in a karst aquifer. The system is taken as a whole to investigate karst spring responses to the rainfall and water surface infiltration process (Dreiss 1982; Barrett and Charbeneau 1996; Zhang et al. 1996).

(2) Approaches involving an analytical model that describes the karst system hydrological functioning. Based on a better understanding of the groundwater flow regime and knowledge of the aquifer parameters, simple hydrological conditions were integrated into a simple analytical expression (Lin and Yang 1988).

(3) Approaches involving a numerical model are the most powerful approaches to study the impact of heterogeneities on the hydraulic parameters and consequently on the karst hydrological functioning. Usually, there are three ways to characterize karst media. The simplest and most commonly used one has been to assume the karst aquifer as an equivalent porous media in which conduit and wide fracture are treated as a high hydraulic conductivity region (Teutsch 1993; Eisenlohr et al. 1997; Scanlon et al. 2003). The second approach is called dual porosity or double permeability model (Mohrlok et al. 1997; Cornation and Perrochet 2002). The basic concept of this approach assumes that the fractured rock consists of two overlapping continua in hydraulic interaction: a matrix continuum of low hydraulic conductivity, primary porosity and a fractured domain with high hydraulic conductivity, secondary porosity (Cornation and Perrochet 2002). The third approach is the coupling of linear flow with nonlinear flow by using the concept of equivalent hydraulic conductivity in the Darcy's law (Cheng and Chen 2004). It is shown that the key to modeling karst groundwater is still dependent on determining an effective approach to couple the conduit flow in the karst channels with the flow in the calcareous formation. These models were generally used to bring a quantitative approach of the pollution transport in the karstic aquifers. The flow equation were usually coupled with the advection-dispersion models to

estimate the flow and transport parameters, such as the mean flow velocity and dispersion coefficient as well as to identify the geometric conduit parameters, such as the conduit volume and diameter (Hauns et al. 2000; Massei et al. 2006; Goldscheider et al. 2007).

Water tracer tests and breakthrough tracer curve (BTC) were used to validate numerical flow-transport models. Tracer tests in karst regions were used to determine the catchment area of a spring and to estimate roughly the characteristics of the fast flow in the conduit network. They were also used to investigate sources of pollution (Ford and Williams 1989). Many studies have presented both fluid flow and solute transport in the karst system to describe the tracer tests. Maloszewski and Hermann (1999) performed two multitracer tests in the major cross fault zones of the Lange Bramke in Germany. They compared the BTC measured with that simulated from the coupling between the advection-dispersion equation and Darcy's law. They showed that the hydraulic conductivity in the fault zone was several orders of magnitude larger than that of the remaining fractured zone of the aquifer. Relationships between the geometry of the karst conduits and breakthrough curves were established by Hauns et al. (2000). They used one dimension advection-dispersion equation to calculate the breakthrough curve using the mean flow velocity. They observed that the dispersion coefficient depended linearly on the average flow velocity in the karst channel under homogeneous flow condition. Other studies about the solute transport in the karst system were carried out using the Darcy's law and multi-porous approach to show that water flow in the conduits was the key parameter to describe the transport in these heterogeneous aquifers (Morales et al. 1995; Couturier and Fourneaux 1998; Rivard and Delay 2004; Massei et al. 2006; Goppert and Goldscheider 2007). However, the Darcy's law was not well adapted to model flow in conduits of large diameter.

In this study, we proposed to use the Darcy's law to describe the water flow within the fractured calcareous bedrock where the pores are small and the Brinkman equation to describe the water flow in the karstic conduits. The latter equation is indeed compatible in the domain where the porosity is high (i.e. > 90%) and thus it enables the description of the fluid flow where velocities are high enough for the momentum transport by shear stress to be important (Brinkman 1947; Durlofsky and Brady 1987; Nield and Bejan 1992; Parvazinia et al. 2006). Brinkman equation was applied to calculate the flow fields in many domains such as in porous squeeze film, in the gaps around the fibber bundles, and in porous heterogeneous materials with more than one typical pore size (Lin et al. 2001; Nicos 2001; Chang and Chen 2003; Albert and Yuan 2004). The present paper proposes to test Brinkman equation to model karstic flows. The first objective of this paper is to describe the water flow in the karst aquifer of the Val d'Orléans by using a two-dimensional numerical model. This model

accounts Brinkman equation within karst channels flow and Darcian flow within the hosting calcareous rock. The second aim is to exploit the flow model results to predict the problem of solute transport in the karst system by using the advection-dispersion equation, and to simulate the tracer transport between the site of injection and the springs. The calibration of the simulation is based on six tracer tests realized for different hydrological conditions. The model established was then used to investigate the role of the drain and the hosting rock parameters on the behaviour of BTCs at the spring points.

Material and method

Study area

The Val d'Orléans is considered as a vast depression of the major bed of the Loire river, 37 km long and from 4 to 7 km wide (Fig. 1). The karst aquifer is hosted within an Oligocene carbonate lacustrine deposit occurring in the center of the Paris basin and called the limestone of Beauce (Guillocheau et al. 2000). This latter formation display variable habit with a significant primary porosity except for micritic facies. This porosity is increased by fracturation and karstification leading to a relative high permeability (5×10^{-11} to 2×10^{-9} m^2) at hectometric scale (Martin and Noyer 2003). The latter is overlapped by the quaternary alluvia of the Loire river.

The Loire river feeds more than 80% of the water hosted in the carbonated karstic aquifer. The estimated inflow of the Loire river in the swallow hole infiltration area of Jargeau varies from 15 to 20 m^3/s and it can reach 100 m^3/s during floods (Chéry 1983). Karst networks are well known in the left bank of the Loire river. The water runs from Jargeau through the karst networks toward the direction of the springs of the Loiret river (Fig. 1) (Zunino 1980; Chéry 1983; Lepiller and Mondain 1986). The springs of this river are called the Bouillon and the Abîme, they are considered as the main emergences of the water lost close to Jargeau in the Loire river (from 0.3 to 5 m^3/s). There are also several smaller springs along the Loiret river as the Béchets, the Saint-Nicolas, the Bellevue and the Pie (Fig. 1). All these springs are surface overflows of the aquifer. The mean aquifer outflow is an underground emergence in the Loire river located around the confluence of Loire-Loiret (Fig.1). Previous studies showed the relation between these springs and the swallow holes points at Jargeau within the Loire river (Zunino 1980; Chéry 1983; Alberic and Lepiller 1998, Lepiller 2001).

Desprez (1967) established the piezometric map of the study area in the periods of low and high waters (more than 700 boreholes). Every year, the difference of water level between the high and low water periods is usually about 1 m. The main drains were located according to the depressions of the piezometric surface and to the previous the different connections derived from all the tracer tests presented in Fig. 1.

Tracer tests

Tracer tests were conducted to study the conduit karst system of the Val d'Orléans. The injection site was located nearby Jargeau 15 km west of the spring of Bouillon (Fig. 1). The tests were performed at 1973, 1998, May 2001, Nov. 2001, 2006 and 2007. 2 kg of uranine diluted with 5 litres of water was injected in May 2001, Nov. 2001, 1 kg on 1998, 2006 and 2007. 15 kg of uranine diluted with 80 litres was injected in 1973 (Table 1). These tests contributed to show the relation between the swallow hole point and the springs system. Fig. 2 shows the tests performed for different hydrological conditions. The datasets recorded the 1973, 1998, May 2001, Nov. 2001, 2006 and 2007 are enable to simulate several configurations about injection protocol and hydraulic condition. Moreover, Fig. 2 shows the variation of the concentration as a function of time, and presents the tracer recovery curves for each spring depending on the existence of sampler to the spring.

Uranine was used for groundwater dye tracing in the karst system of the Val d'Orléans because of its great sensitivity of detection and its weak tendency to adsorption. Tracer was analysed by mean of fluorescence spectrofluorimetry (Hitachi 2000, Hitachi 2005, and Turner). The excitation and emission for uranine were 250 and 500 nm, respectively.

For the tracer test, uranine was injected in the swallow hole point at Jargeau, and it was detected at the springs on the Loiret river. Samples were taken automatically at each spring point from 1.5 m depth of the spring water surface. During this excitation, a fluorescent light is emitted. This fluorescent is proportional to the dye concentration (SSH 2002). Table (1) show the details for each uranine tracer testes at Jargeau such as the samples number which have been collected at the spring point, sampling frequency, tracer mass injected at the swallow point, and the limits of detection for the spectrofluorimeter.

The BTC enables the calculation of several parameters related to the transit time and velocity (leading edge, trailing edge and peak velocity), to the tracer concentration (maximum and average), and to the duration of the recovery (Table 2). Times are measured by taking the injection time (t=0) as reference. The distance used for calculation of velocities is the straight line between the injection site and the sampling point. Consequently, the values obtained for velocity are minimum values, the real values depending on the tortuousness of the drains (Worthington 1999; Field and Nash 1997) and being from 1.3 to 1.5 times higher (Field 1999; Field and Pinsky 2000). The curve of the tracer mass flow rate enabled the calculation of the mass of the tracer recovery. The ratio between this mass recovered and the initially injected mass is the recovery rate.

The Residence Time Distribution (RTD) is obtained by relating the mass flow to the recovered tracer mass (Table 2). It has inverse time units and represents the probability density function that a traced water

element stays in the system for a time between t and t+dt (Molinari 1976). The variance of the residence time is an indication of the dispersion around the means residence time. There is no mixing if the variance nears to zero and complete mixing if the variance tends toward infinity. All parameters which can be calculated from the tracer test are shown in Table 2.

Development of the coupled model

In the light of the previous description of the karst system with flowing within a fractured porous aquifer and karst channels it is necessary to find an adapted mathematical model describing the water flux and solute transport between swallow holes and springs.

Darcy's law

The Darcy's law describes fluid flow in porous media and it is well adapted to an aquifer with small porosity. This equation describes the flow behaviours in porous media as driven by pressure gradients as following:

$$u_D = -\frac{k_D}{\mu}\nabla p \qquad (1)$$

where u_D is the Darcy flow velocity (m/s), k_D the intrinsic permeability related to the Darcy's law (m²), μ the fluid viscosity (Pa.s) and p the pressure (Pa).

Brinkman equation

The Brinkman equation describes the fluid flow in porous media where velocities are high with no-negligible momentum transport by shear stress. In the Darcy model, it is effectively assumed that all stress within the flow is negligible compare to the stress carried by the interface of the liquid solid porous media. This assumption cannot be regarded to be physically realistic for high permeability porous media where at least part of the viscous stress is limited within the fluid domain. The Brinkman equation, which accounts for the transition from Darcy flow to viscous free flow, is ideal to be used for high permeability porous regimes (Brinkman 1947; Parvazinia et al. 2006). This equation is adapted to describe the flow in porous media if the porosity is greater than 90% (fast flow) (Durlofsky and Brady 1987). The Brinkman equation for steady state flow is:

$$u_{Br} = \frac{k_{Br}}{\mu}\left[-\nabla p + \mu_e \nabla^2 u_{Br}\right] \qquad (2)$$

$$\nabla u_{Br} = 0$$

where u_{Br} *is* the Brinkman fluid velocity (m/s), μ the fluid viscosity (Pa.s), k_{Br} the intrinsic permeability related to Brinkman equation (m^2), μ_e the effective viscosity that theoretically takes into account the stress within the fluid as it flows through a porous medium. However experimental measurement of μ_e is not trivial (Nield and

Bejan 1992). Therefore, in the present work in accordance with the published literature, μ_e is set to be equal to the fluid viscosity μ (Hsu and Cheny 1985; Kaviany 1986; Allan and Hamdan 2002; Parvazinia et al. 2006). In the following part, the $_D$ and $_{Br}$ indices the Darcy's law and Brinkman equation, respectively as the model deals with the two flow equations.

Solute transport equation

This equation describes the migration of chemicals in multi-porous media. The phenomenons which govern the solute movement are advection and dispersion. They are described by the solute transport equation as following:

$$\theta \frac{\partial c}{\partial t} + \nabla u.c = \nabla \left[D \nabla c \right] + Q \qquad (3)$$

where c is the solute concentration (kg/m^3), θ the media porosity, D the hydrodynamic dispersion tensor (m^2/s), u the velocity vector (m/s) originating the Darcy's law or Brinkman equation, and Q the source term (kg/m^3.s). In this equation, the first term describes the concentration change with time and the second term is the advection term, and the first term on the right hand is the hydrodynamic dispersion of concentration.

The advection describes the transport of solute, such as a pollutant at the same velocity of the groundwater flow. Hydrodynamic dispersion in a porous medium occurs as a consequence of two processes: (1) molecular diffusion which originates from the random molecular motion of solute molecules, and (2) mechanical dispersion which is caused by non-uniform velocities and flow path direction. Molecular diffusion and mechanical dispersion cannot be separated in a flow regime (Bear 1979) and the summation of these two coefficients is called the hydrodynamic dispersion. The hydrodynamic dispersion tensor for isotropic porous media is defined in the following x-y components form as following:

$$D_{xx} = \alpha_L \frac{u^2}{|u|} + \alpha_T \frac{v^2}{|u|} + D_m$$

$$D_{yy} = \alpha_L \frac{v^2}{|v|} + \alpha_T \frac{u^2}{|v|} + D_m \qquad (4)$$

$$D_{xy} = \left[\alpha_L - \alpha_T \right] \frac{uv}{|u|}$$

where D_{ii} are the principal components of the hydrodynamic dispersion tensor (m^2/s), α_L the longitudinal dispersivity coefficient (m), which is parallel to the direction velocity, α_T the transverse dispersivity coefficient (m), D_m the effective molecular diffusion coefficient ($\approx 10^{-9}$ m^2/s), u and v components of the velocity vector along the x,y direction originating from the Darcy's law or Brinkman equation.

Coupling

The two flow equations in this work are fundamentally compatible since both describe fluid velocities and pressure distributions. The depended variable in Darcy's law is the pressure alone, whereas pressure and direction velocities are the dependent variables in the Brinkman equation. The analysis begins by a hydrodynamic model using the Darcy's law in porous massif limestone and Brinkman equation in the karst channels. Next, the model examines the tracer transport in the karst system by coupling the solute transport equation with the Darcy's law and Brinkman equation.

Geometry and boundary conditions

The application of the hydrodynamic-transport model is used to simulate a reach of 24 km from the site of Jargeau down to the confluence Loire-Loiret. It is based on a two dimensional (x,y) description of the hydrogeological system. This simulation consider the water table as a boundary condition, thus well extractions and the effect of infiltrated precipitation in the karst aquifer are considered as constant parameters, that keep the water table stable (Chéry 1983; Lepiller and Mondain 1986).

The location of the karstic drain between Jargeau and the spring points of Loiret river until the confluence of Loire-Loiret was deduced from the piezometric lines describing a valley at the piezometric surface. These linear depressions suggest the presence of karstic drains. Therefore, two hydrodynamic domains could be defined: (1) a Darcy domain where the piezometric map is not perturbed, and (2) a Brinkman domain in the karstic channel which size will be discussed below.

In both domains, the pressure variation was deduced from the piezometric maps and adapted for simulation during low and high waters periods. These pressures were used as boundary condition for the Darcy and Brinkman domain, as following:

$$p = \rho g\left(H - H_o\right) \tag{5}$$

where p is the pressure of each water isoline, H the water level isoline (m), and H_o the reference water level isoline (m). For a continuous solution across the interface between the zone of Darcy and Brinkman flow, the pressure from Darcy's law equalled the pressure from the Brinkman equation, use the following constrain on pressure for the Darcy- Brinkman interface:

$$p_D = p_{Br} \tag{6}$$

The boundary conditions at the extern zones surrounding the study area are symmetry, i.e. the integrated flow velocity on this boundary is zero.

For the Brinkman flow in the karst channels, the pressures at the swallow holes and spring points take the direct values, for the swallow holes points (points 1, 2 and 3) the pressures were 88200, 49250 and 49000 Pa, respectively. The pressure value for the swallow hole points area (fig. 3) is 93100 Pa, and for the spring points which discharge in the Loire river (points 4, 5 and 6) the pressures were -550, -2600 and -3425 Pa, as shown in Fig.3. This figure shows the boundary conditions for the Darcy-Brinkman model.

To compare tracer recovery realised on field and simulation, the transport equation is solved using the velocity given in the Darcy and Brinkman domain. At t_0 the tracer concentrations is everywhere equal to zero except at injection site where the concentration equals to initial concentration injected. The continuity tracer flux is carried out in the Darcy domain where tracer is transported. At the Darcy-Brinkman interface, the tracer concentrations are equal, and advective flux condition is taken for the spring points and the boundaries of the study area.

Once defined the boundary in the fluid flow model, the boundary conditions are mix of Dirichlet, Neumann and Cauchy conditions.

Results and discussion

Tracer tests

The amount of the tracer recovery at the spring is highly variable according to the hydrological conditions, the amount of tracer mass injected, and the circulating flow rate. The percentage of tracer recovery increases at the spring in conditions of low waters and with the increasing mass of tracer injected.

The tracer was first detected at the spring of Bouillon 70, 84, 74, 81, 72 and 57 hr after the tracer injection at 1973, 1998, May 2001, Nov. 2001, 2006 and 2007, respectively. The uranine concentration reached its maximum of 5.91 ng/ml after 92 hr for the test of the 1973, 0.56 ng/ml after 100 hr for the test of the 1998, 0.39 ng/ml after 87 hr for the test of the May 2001, 0.56 ng/ml after 104.5 hr for the test of the Nov. 2001, 0.072 ng/ml after 88 hr for the test of the 2006 and 0.1 ng/ml after 79 hr for the test of the 2007. These differences will be investigated thank to the parametric tests of the proposed model developed in the discussion. Table 3 gives the different characteristic values for the six tracer tests with injection at Jargeau and recovery at the spring of Bouillon (Lepiller and Mondain 1986).

First calibration of hydrodynamic parameters

The model describes the transport of tracer in karst aquifer, the fluid flow and solute transport equations are solved using the commercial COMSOL multiphysics software. The model area is divided into a triangle plane mesh in each aquifer with a total numbers of elements and nodes of 67300 and 33897, respectively.

To generate the tracer transport model, we have to follow the following two steps. First, the steady state water flow is generated and a stable hydrodynamic solution is stored. In the second step, this result is injected to solve the solute transport equation and to follow the transient migration of the tracer.

The result produces by the model needs to be calibrated, and a first step is necessary to estimate roughly the hydrodynamic parameters. The validity of the model is based on the comparison with the velocity flow rates recorded during tracer tests (0.04-0.06 m/s). In the domain of Brinkman (karst channels), the principal parameters are the drain size and the permeability. In the domain of Darcy (low porosity), the permeability is the main parameter that control flow and it is assumed constant.

Channel diameter

The behaviour of the mean velocity in the karst channels in case of steady state flow with different drain diameters as a function of hydraulic parameters is presented in Fig. 4. Generally, in the karst channel the means velocity increases with diameter decreases and with permeabilities. The diameter of the drain does not influence the mean velocity when the permeability of the fractured zone is very low (Fig. 4a). The influence of the Brinkman permeability for drain of 5 m and 10 m diameter is not significant (Fig. 4b). The diameter of the channels observed by the speleologists between the swallow hole points at Jargeau and the spring points of Loiret river varies between 2 m and 10 m, therefore a diameter of 5 m provided the best results compared with the mean velocity measured in the channels by the tracer tests.

Permeability

The best results are achieved when the Darcy permeability varies from 8×10^{-11} to 6×10^{-10} m^2 and the Brinkman permeability varies from 5×10^{-6} to 5.5×10^{-5} m^2. Fig.5 shows the results of the hydrodynamic model in case of steady state flow for low water levels. The mean velocity obtained in the drains is 0.05 m/s and in the fractured zone is 1.35×10^{-6} m/s. Calculation for high waters levels show that the mean velocity obtained in the drains is 0.06 m/s and in the fractured zone is 1.45×10^{-6} m/s.

These results clearly show that the velocity in the domain of Brinkman is greater than that in the domain of Darcy. This can be attributed to the effect of shear stress and the high permeability in the Brinkman equation.

The velocity field in the domain of Darcy is almost uniform, but it increases radically in the zone where pressure gradient is higher.

Simulation of tracer transport (steady and unsteady problem)

One week is needed for the tracer to reach from the injected point to the spring. During this period, the variation of flow rate could be evaluated by the variations of water levels with the time in the Loire river. The water levels of the Loire river at the Orléans Bridge during the tracer testes are shown in Fig. 6a, b, c, d, e and f. In general, the water level variation is lower than 0.3 m. Chéry 1983; Lepiller and Mondain 1986 denoted that the variation of flow rate in springs is negligible during the period of tracer transport. Therefore, hydrodynamic equations are solved for the steady state. Flow and velocity field is generated in the domains of Darcy and Brinkman, these solutions are injected in the solute transport equation.

To simulate tracer transport it is necessary to solve the transport equation for temporal model, i.e. for unsteady state. The analysis period is 10 days and the output times setting are simulated by means of similar vectors of times starting at zero with step of 2 hours up to 10 days. The parameters that must be adjusted in the hydrodynamic-transport model include permeabilities and dispersivity coefficients in the domain of Darcy and Brinkman.

The resolution of this transient problem allows the plotting of the breakthrough curves (BTCs) corresponding to the tests considered. The fitting between breakthrough curves and experimental data is evaluated by assessing the magnitude of the error generated. To compare the results obtained by the model, six tracer testes are chosen which were conducted during low and high waters periods.

Sensitivity of the model to the main parameters

Several simulations of tracer recovery are compared to the six tracer tests presented before. In these simulations, the Darcy and Brinkman permeabilities are constant and the Boundary condition is given by piezometric map of low water period except for the tests of 1973, 2006 and 2007 that were performed during high water period, using the high water piezometric map.

Many parameters influence the tracer transport process, such as permeabilities, longitudinal and transverse dispersivity coefficients in the domain of Darcy and Brinkman, the level of the water table and the mass tracer injected. Therefore, it is important to study the effect of the variations of these parameters separately to describe the rate and pattern of transport and hierarchies their influences, which occurs after injection.

Permeability

The comparison between theoretical BTC curves for different values of Darcian permeability (Fig. 7a) show the decrease of tracer concentrations recovery with permeability increases. Thus, the increasing of Darcy velocity leads to an increasing of the tracer concentrations toward the domain of Darcy. At the opposite, the increase in the Brinkman permeability increases the mean velocity in the channels and consequently the tracer concentrations (Fig. 7b).

Dispersivity

The dispersivity coefficients play a significant role in the behaviour of the tracer transport. These coefficients are affected by the mean velocity in the domain and the karst geometry of the domain (Majid and Leijnse 1995; Gaganis et al. 2005; Faidi et al. 2002; Ham et al. 2004). Concerning the problem of transport, we noticed that authors who used the equation of transport in the porous media were forced to apply different values for the ratio α_T / α_L (Younes et al. 1999; El-Mansouri et al. 1999; Kim et al. 2003; Ham et al. 2004). In open channels, Mohan and Muthukumaran (2004) found that the best value for α_T / α_L ratio was 1 when they simulated the pollutant transport in the river bed. In our study, this ratio equal to 1 in the drains (free flow).

A good agreement is obtained when $\alpha_L = \alpha_T$ whatever the domain. Herein, four values were examined ($\alpha_L = \alpha_T$ = 40, 50, 60 and 70 m in the domain of Brinkman and $\alpha_L = \alpha_T$ = 5, 15, 25 and 35 m in the domain of Darcy). From Fig. 7c, when the dispersivity coefficients in the domain of Brinkman increase, the recovery of tracer concentration decrease. This because the tracer dispersion toward the fractured zone increases when these coefficients increase. Reducing the dispersivity coefficients in the domain of Darcy causes an increase of tracer concentrations (Fig. 7d). The increase of dispersivity coefficients in the domain of Darcy causes an increase in concentrations levels in this domain and, consequently, decrease in the concentrations levels at the spring of Bouillon.

Piezometric surface

The effect of water level change on the behaviour of tracer recovery at the spring of Bouillon is shown in Fig. 7e. This figure show four different values of water level at Jargeau (h=96.5, 97, 97.5 and 98 m). It can be clearly seen that when the water level along the study area increases, we will find low tracer recovery at the spring. This can be attributed to the effect of tracer dispersion toward the fractured zone which increases with the water level. This suggests an important dilution during high water period.

Mass tracer injected

The injected mass influences the maximum tracer concentration at the spring as shown in Fig. 7f, when the injected mass increases, the concentration of tracer recovery increases, and the testes of the 1973 and 2007 confirm this because the injected mass for the test of the 1973 was 15 kg and it was 1 kg for the test of the 2007. This can be caused to the dilution process.

Table 4 summarises the effect of hydrodynamic-transport parameters on the tracer recovery parameters (mean residence time (MRT), time recovery (t_1), recovery rate (R%) and variance).The hydrodynamic transport parameters are the permeabilities and dispersivity coefficients. This table shows that all tracer recovery parameters are influenced by the variations of hydrodynamic-transport parameters but not with the same magnitude, because it can be observed that the permeability and the ratio between the longitudinal and transverse dispersivity coefficients influence strongly on the tracer recovery parameters. Moreover, the water level along the study area influences the mean residence time and R%.

Best fitting

The optimum numerical solution is shown in Fig. 8, which compares the concentrations simulated to that measured BTCs at the spring of Bouillon, the spring of the Pie, the spring of Béchets and the spring of Saint Nicolas. From this figure, it can be found that the predicted times recovery are slightly lower than that measured, this can be attributed to the 2 hours time accuracy of our model. Moreover, this figure yields the best fitting corresponding to that measured BTC thanks to the calibration processes which yield a permeability of 5.6×10^{-10} m^2 in the domain of Darcy, and in the domain of Brinkman the best permeability was 1.65×10^{-5} m^2 between Jargeau and the spring of Bouillon, and 5.5×10^{-5} m^2 between the spring of Bouillon and the confluence Loire-Loiret. These calibrated data present a linear relation with the measured flow rate at the spring of Bouillon. Finally, the best fitting is realised when the $\alpha_L = \alpha_T = 5$ m in the domain of Darcy for the tests of 2006, May 2001, Nov. 2001, 1998 and 1973, and equal to 1 m for the test of 2007. In the domain of Brinkman, $\alpha_L = \alpha_T = 43$ m for the test of 2007, 28 m for the test of 2006, 53 m for the test of Nov. 2001, 23 m for the test of May 2001, 50 m for the test of 1998 and 20 m for the test of 1973.

Table 5 presents a summary of measured and predicted tracer parameters for each tracer tests at the spring of Bouillon. It can be found that the calculated water flow at the spring is near to that measured and the predicted tracer parameters are very near to that measured with different hydrological conditions.

Conclusion

We have presented an adapted model to estimate the solute transport in the karstic aquifer. In this model, the water flows in the channels are governed by the Brinkman equation, because this equation is indeed compatible in the domain where the porosity is high (> 90%) and thus enables description of the fluid flow in the karst channels where velocities are high enough for the momentum transport by shear stress to be important. Darcy law was used to describe the water flow in the surrounding rocks. These domains are connected through their boundary condition where a continuous pressure is assigned.

The hydrodynamic analysis allows to generate the solute transport model with the aim of analyzing the uranine tracer transport in the karst aquifer of the Val d'Orléans. COMSOL multiphysics finite element analysis software was used to solve the governing equations. Six tracer tests were employed to investigate the accuracy of the calculated results. The calibration of the model indicates that an agreement is obtained between calculated data and that experimental test when the draining permeability (Brinkman permeability) ranges from 5×10^{-6} to 5.5×10^{-5} m^2, the limestone permeability (Darcy permeability) ranges from 8×10^{-11} to 6×10^{-10} m^2. A 5 m diameter of the channel represented a suitable results compared to that measured. Finally, a good result is obtained when the dispersivity coefficients in the drains is isotropic and ranges from 23 to 43 m in the fractured zone with a thickness between 1 to 5 m.

Acknowledgements

We would like to think Professor M.Motelica for improving the English language. Thanks are also extended to "Centre National des Oeuvres Universitaires et Scolaires" for the financial support during the research period.

References

Alberic P, Lepiller M (1998) Oxydation de la matière organique dans un système hydrologique karstique alimenté les pertes fluviales (Loiret, France). Water Resour Res 32(7):2051-2064

Albert S, Yuan R (2004) Hydrodynamics of an ideal aggregate with quadratically increasing permeability. J Colloid and Interface Science 285:627-633

Allan FM, Hamdan MH (2002) Fluid mechanics of the interface region between two porous layers. Appl. Math. Comp 128:37-43

Bear J (1979) hydraulics of groundwater. McGraw-Hill New York

Barrett ME, Charbeneau RJ (1996) A parsimonious model for simulation of flow and transport in a karst aquifer. Center for Research in Water Resources, Technical Report 269, p 149

Brinkman HC (1947) A calculation of the viscous force exerted by a flowing fluid on a dense swarm of particle. Appl.Sci. Res. A1 27-34

Chang C (2003) Tow impregnation of unidirectional fibrous perform during resin transfer molding. J Reinforced Plastics and Composites 22:1003-1016

Cheng JM, Chen CX (2004) An integrated linear/non-linear flow model for the conduit-fissure-pore media in the karst triple void aquifer system. Environmental Geology 47:163-174

Chéry JL (1983) Etude hydrochimique d'un aquifère karstique alimenté par perte de cours d'eau (la Loire). PhD Thesis, Orléans University

COMSOL Multiphysics (2006) Earth –Sciences module model library

Cornation F, Perrochet P (2002) Analytical 1D dual porosity equivalent solution to 3D discrete single continuum models. Application to karstic spring hydrograph modelling. J Hydrol 262:165-176

Couturier B, Fourneaux J (1998) Les relations karst rivière dans les calcaires bédouliens du Diois (Drôme France) exemple de la Gervanne. Bull Eng Geol Env 57:207-212

Desprez (1967) Inventaire et étude hydrogéologique du Val d'Orléans (Loiret). BRGM DSGR 67 A 21.16

Dreiss (1982) Linear Kemels for karst aquifers. Water Resources 18(4):865-876

Durlofsky L, Brady JF (1987) Analysis of the Brinkman equation as a model for flow in porous media. Phys. Fluids 30:3329-3341

Eisenlohr L, Bouzelboudjen M, Kiraly L, Rossier Y (1997). Numerical versus statistical modelling of natural response of a karst Hydrogeological system. J Hydrol 202:244-262

El-Mansouri B, Loukili Y, Esselaoui D (1999) Une approche numérique des périmètres de protection des captages des eaux souterraines. Comp. Rend. Acad. Sc . Paris, Série II a 328:695-700

Faidi A, Garcia L, Alberlson M (2002) Development of a model for simulation of solute transport in a stream-aquifer system. Environmental Modelling and Assessment 7(3):191-206

Field MS (1999) The Qtracer programme for tracer breakthrough curve analysis for karstic and fractured rock aquifers. United States Environmental Protection Agency, Washington, D.C., Publication EPA/600/R-98/156a, 137 p

Field MS, Nash SG (1997) Risk assessment methodology for karst aquifer. Environ. Monitor. Assess, 47:1-21

Field MS, Pinsky PF (2000) A two regions non equilibrium model for solute transport in solution conduits in karstics aquifer. J Hydrol 44:329-351

Ford DC, Williams PW (1989) Karst geomorphology and hydrology. Unwin Hyman, London, 601 p

Gaganis P, Skouras ED, Theodoropoulan MA (2005) On the evaluation of dispersion coefficients from visualization experiments in artificial porous media. J Hydrol 307:79-91

Goldscheider N, Meiman J, Pronk M, Smart C (2007). Tracer testes in karst hydrogeology and speleology. J International of Speleology 37(1):27-40

Goppert N, Goldscheider N (2007) Solute and colloid transport in karst conduits under low and high flow conditions. J Groundwater 46:61-68

Guillocheau F, Robin C, Allemand P, Bourquin S, Brault N, Dromart G, Friedenberg R, Garcia J, Gaulier J, Gaumet F, Grosdoy B, Hanot F, Le Strat P, Mettraux M, Nalpas T, Prijac C, Rigollet C, Serrano O, Grandjean G (2000). - Meso-Cenozoic geodynamic evolution of the Paris Basin: 3D stratigraphic constraints Geodin. Acta 133(4):189-246

Ham PAS, Schotting RJ, Prommer H, Davis GB (2004) Effects of hydrodynamic dispersion on plume lengths for instantaneous bimolecular reactions. Adv. Water Resour 27(8):803-813

Hauns M, Jeannin PY, Aheia O (2000) Dispersion, retardation and scale effect in tracer breakthrough curves in karst conduits; J Hydrol 241:177-193

Hsu CT, Cheng P (1985) The Brinkman model for natural convection about a semi-infinite vertical flat plate in a porous medium. Int. J Heat Mass Transfer 28:663-97

Kaviany M (1986) Non-Darcian effects on natural convection in porous media confined between horizontal cylinders. Int. J. Heat mass Transfer 29:1513-1519

Kim S, Hyeok K, Dong-Ju Kim, William A (2003) Determination of two-dimensional laboratory scale dispersivities. Hydrol.Process 18:2475-2483

Lepiller M, Mondain PH (1986) Les traçages artificiels en hydrogéologie karstique. Hydrogéologie 1:33-52

Lepiller (2001) Traçages appliqués à la dynamique des aquifères karstiques. Géologue 129 : 79-84

Lin J, Lu R, Yang C (2001) Derivation of porous squeeze-film Reynolds equations using the Brinkman model and its application. J Phys. D:Appl.Phys 34:3217-3223

Lin M, Chen CX (1988) Analytical models of groundwater flows to the karst springs. In: Yuan DX (ed) karst hydrology and karst environmental protection, Proceeding of the 21st IAH congress, Wallingford, Oxfordshire, IAHS spec Publ No. 176 1(2):647-654

Majid S, Leijnse A (1995) A non linear theory of high concentration gradient dispersion in porous media. Adv. Water Resour 18(4):203-215

Maloszewsky P, Hermann A (1999) Interpretation of tracer tests performed in fractured rock of the Lange Bramke basin, Germany. J Hydrol 7:209-218

Martin JC, Noyer ML (2003) Caractérisation du risque d'inondation par remontée de nappe sur le Val d'Orléans. Etude hydrogéologie, BRGM

Massei N, Wang HQ, Field M (2006) Interpretation tracer breakthrough tailing in a conduit dominated karstic aquifer. J Hydrogeol 14:849-858

Meus P (1993) Hydrogéologie d'un aquifère karstique dans les calcaires carbonifères. Apports des traçages à la connaissance des milieux fissurés et karstiques. Ph.D. Thesis, Liège University

Mohan S, Muthukumaran M (2004) Modelling of pollutant transport in groundwater. IE (I) Journal-EN. pp. 22-32

Mohrlok U, Kienle J, Teutsch G (1997) Parameter identification in double-continuum models applied in karst aquifers. Proceedings of the 12th International Congress of Speleology 2:163-166, Switzerland

Molinari J (1976) Perspectives offertes par l'utilisation rationnelle des traceurs naturels et artificiels en hydrologie karstique. Commentaires de nombreux exemples récents de multitrac¸ages [On the use of natural and artificial tracers in karst hydrology: some comments of recent examples of multitracing experiments]. Ann. Sci. Univ Besanc¸on Geol 25:275–306

Morales T, Oazar M, Arandes J, Zafra P, Antiguedad I, Basauri F (1995) Application of a solute transport model under variable velocity conditions in a conduit flow aquifer : Olalde karst system, Basque contry, Spain. J Environmental Geology 30:143-151

Nicos S (2001) Improved approximation of the Brinkman equation using a lattice Boltzmann method. Phys. Fluids 13:1807-1810

Nield DA, Bejan A (1992) Convection in porous media. New York: Soringer-Verlag

Parvazinia M, Nassehi V, Wakeman RJ (2006) Finite element modelling of flow through a porous medium between two parallel plates using the Brinkman equation. Transport in Porous Media 63:71-90

Rivard C, Delay F (2004) Simulations of solute transport in fractured porous media using 2D percolation networks with uncorrelated hydraulic conductivity fields. J Hydrogeol 12:613-627

Scanlon B, Mace R, Barrett M, Smith B (2003). Can you simulate regional groundwater flow in a karst system using equivalent porous media? Case study, Barton Springs Edwards aquifer, USA. J Hydrol 276:137-158

Shirley JD (1989) Regional scale transport in karst aquifer. Water Resources 25(1):126-134

Smart C (1988) Artificial tracer techniques for the determination of the structure of conduit aquifers. Ground Water 26(4):445-453

Société suisse hydrogéologie (SSH), Group de travail. Utilisation des traceurs artificiels en hydrogéologie. Rapport de l'OFEG, Série Géologie, n^{o} 3. Berne : SSH, 2002.

Teutsch (1993) An extended double porosity concept as a practical modelling approach for a karst terrain. In: Cutekin G, Johnson AI, Back W (eds) Hydrogeological processes in karst terrains. Processing. Antalya Symposium and Field Seminar, IAHS Spec. Publ. 207:281-292

Worthington SRH (1991) Karst hydrology of the Canadian rocky mountains. Ph.D, McMaster University, Ontario, Canada, pp. 380

Younes A, Ackerer P, Mose R (1999) Modeling variable density flow and solute transport in porous medium: 2. Re-evaluation of the salt dome flow problem. Transport in Porous Media 35:375-394

Zhang YK, Bai EW, Libra R, Rowden R, Liu H (1996) Simulation of spring discharge from a limestone aquifer in Iowa. J Hydrogeol 4:41-54

Zunino (1979) Contribution à l'étude hydrogéologique du Val d'Orléans. Ph.D. Thesis, Orléans University

Figure captions

Fig. 1 Underground waters karstic circulations of the Val d'Orléans (Lepiller and Albéric 1998)

Fig. 2 **a** Tracer tests at 6/02/1973, **b** Tracer tests at 20/02/1998, **c** Tracer tests at 25/05/2001, **d** Tracer tests at 15/11/2001, **e** Tracer tests at 16/11/2006 and **f** Tracer tests at 14/11/2007

Fig. 3 Darcy-Brinkman boundary setting for the low waters periods

Fig. 4 Mean velocity in the drain **a**. as the function of fractured zone permeability, **b**. as the function of draining permeability.

Fig. 5 Water flow for steady state solution. Surface plot represents the pressure distribution (Pa), and arrow plot represents the velocity of Brinkman (m/s) with permeability in the domain of Darcy=5.6× 10^{-10} m^2 and the permeability in the domain of Brinkman=1.65× $10^{-5}m^2$.

Fig. 6 Water level for the Loire river at the Orléans Bridge **a** February 1973, **b** from 13 February to 10 March 1998, **c** from 16 May to 11 Jun 2001, **d** November 2001, **e** from 9 November to 25 November 2006, **f** from 3 November to 24 November 2007

Fig. 7 The effect of Hydrodynamic-transport parameters on the behaviour of BTC at the spring of Bouillon, **a** behaviour of BTC curve (draining permeability=1.65×$10^{-5}m^2$, α_D =5m and α_{Br} =53m), **b** behaviour of BTC curve (Fractured permeability=5.6×$10^{-10}m^2$, α_D =5m and α_{Br} =53m), **c** behaviour of BTC curve (draining permeability=1.65×$10^{-5}m^2$, fractured permeability=5.6×$10^{-10}m^2$, α_D =5 m), **d** behaviour of BTC curve (draining permeability=1.65×$10^{-5}m^2$, fractured permeability=5.6×$10^{-10}m^2$, α_{Br} =53m), **e** behaviour of BTC curve as a function of water level (draining permeability=1.65×$10^{-5}m^2$, fractured permeability=5.6×$10^{-10}m^2$, α_D =5m and α_{Br} =53m,), **f** behaviour of BTC curve as a function of injection time (draining permeability=1.65×$10^{-5}m^2$, fractured permeability=5.6×$10^{-10}m^2$, α_D =5 m and α_{Br} =53m,).

Fig. 8 Comparison between simulated and measured BTCs for the tracer testes when draining permeability =1.65×$10^{-5}m^2$ between Jargeau and the spring of Bouillon, and 5.5×10^{-5} m^2 between the spring of Bouillon and the confluence Loire-Loiret, fractured permeability =5.6×10^{-10} m^2. **a** test 6/02/1973, **b** test 20/02/1998, **c** test 25/05/2001, **d** test 15/11/2001, **e** test 16/11/2006, **f** test 14/11/2007.

Table captions

Table 1 Principles informations of tracer tests realized at Jargeau

Table 2 Parameters obtained from the data a carried out tracer test

Table 3 Parameters obtained by the tracer tests for the spring of Bouillon

Table 4 Summarise the effect of hydrodynamic-transport parameters on the tracer recovery parameters

Table 5 Comparison between predicted and measured tracer test parameters at the spring of Bouillon


Avril 2000
FOREST ofORLEANS
ORLÉANS
Loire River
Bellevue
St Nicolas
Loiret River
The Pie
the Béchets
89m
88m
90m
91m
92m
93m
GLACIS of OLIVET
The Abîme
The Bouillon
Dhuy
Jargeau
Châteauneuf
sur-Loire
Sandillon
The Arche
Chart of karstic circulations of Orleans Valley
Michel Lepiller, Bruno Leclerc
Laboratory of Hydrogeology, Orleans university
Patrick Albéric
ISTO, CNRS - Orleans university
Philippe Boismoreau, Jacques Munerot
Subaqueous speleology Loiret
Alluvial formation of old indifference
Burdigalien : argillaceous formation sablo of the sologne and Orleanais (littel permeable)
Aquitanien : Limestone of Beauce (permeable)
Limestone of Beauce under alluvial cover
Swallow hole point
Perenneial spring point
Swallow hole-spring point
Absorbing drilintg
Drilling (Drinking water supply)
Littel fonctional valley
Connection highlighted by tracing
Piezometric lines (low waters period)
0
5 Km

Figure 1

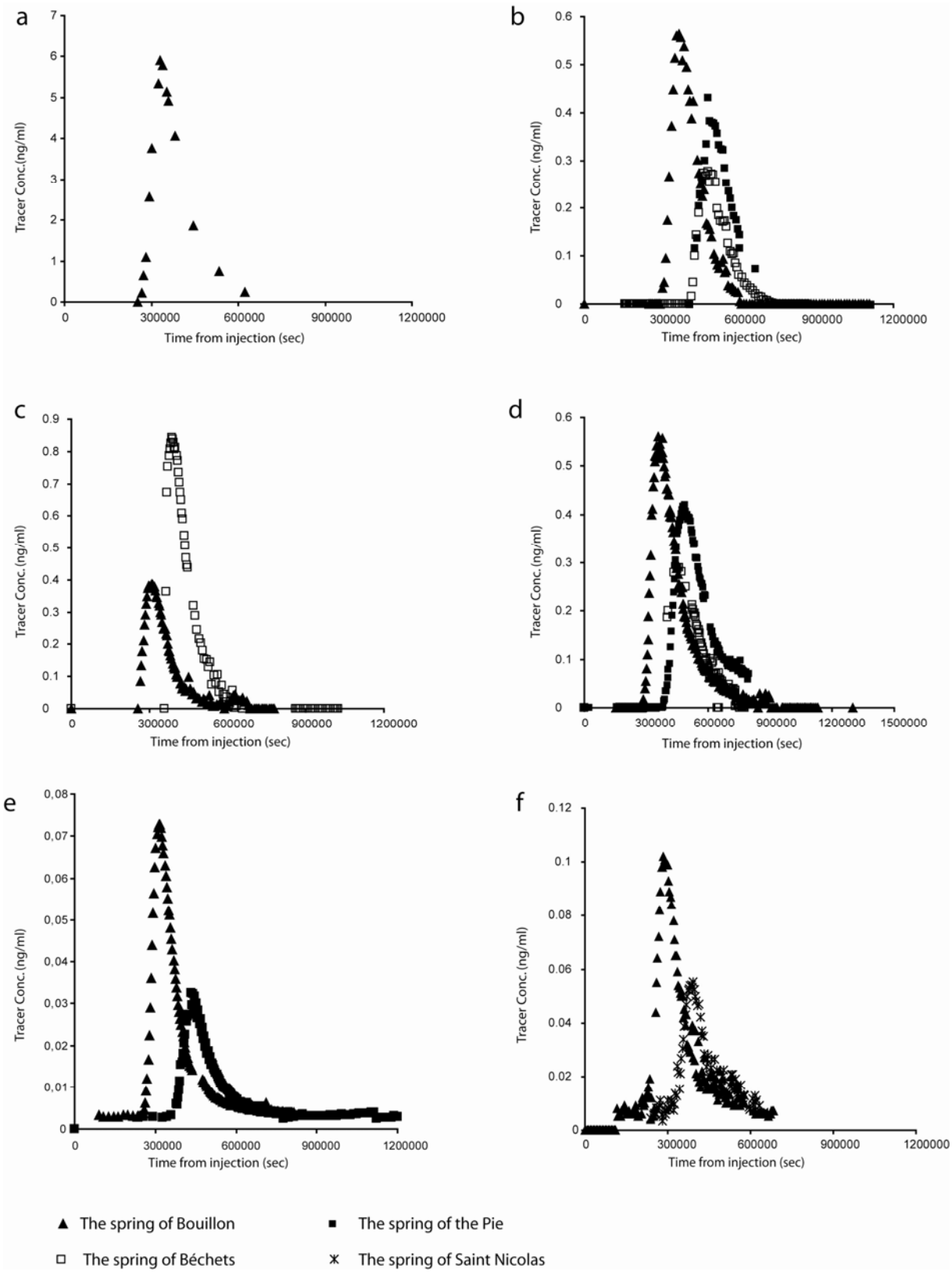
a
b
c
d
e
f
Tracer Conc.(ng/ml)
Tracer Conc. (ng/ml)
Time from injection (sec)
0
300000
600000
900000
1200000
1500000
The spring of Bouillon
The spring of the Pie
The spring of Béchets
The spring of Saint Nicolas

Figure 2

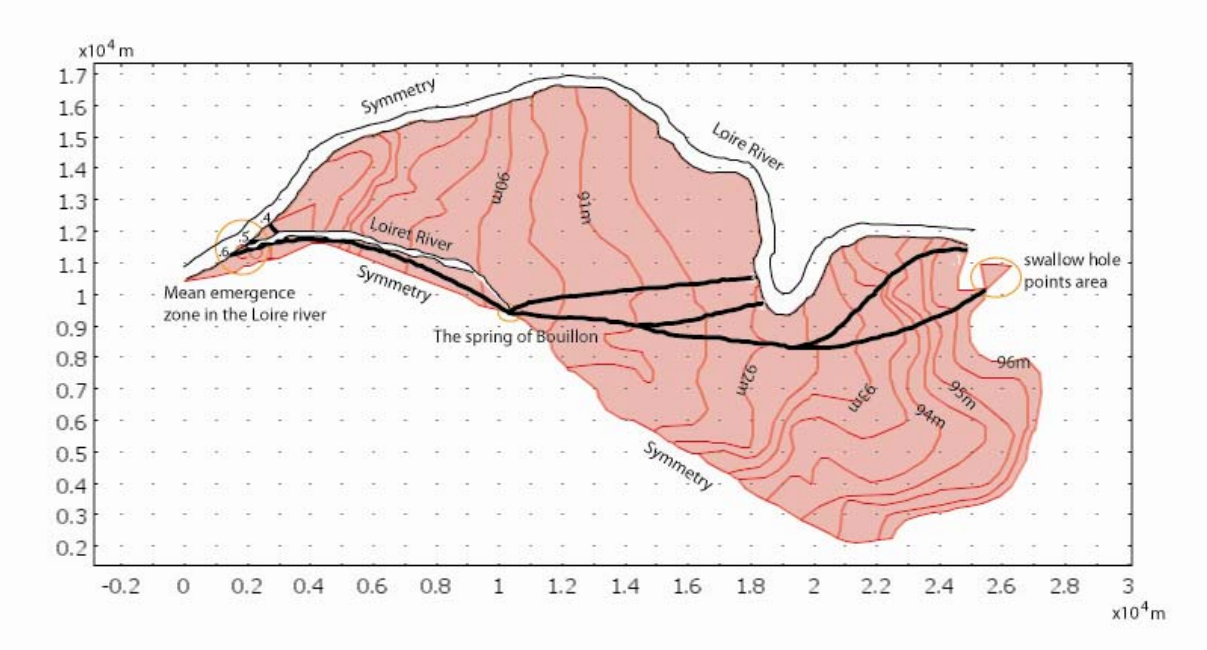
x10^4 m
Symmetry
Loire River
Loiret River
Symmetry
Mean emergence
zone in the Loire river
The spring of Bouillon
swallow hole
points area
90m
91m
92m
93m
94m
95m
96m
Symmetry
x10^4 m

Figure 3

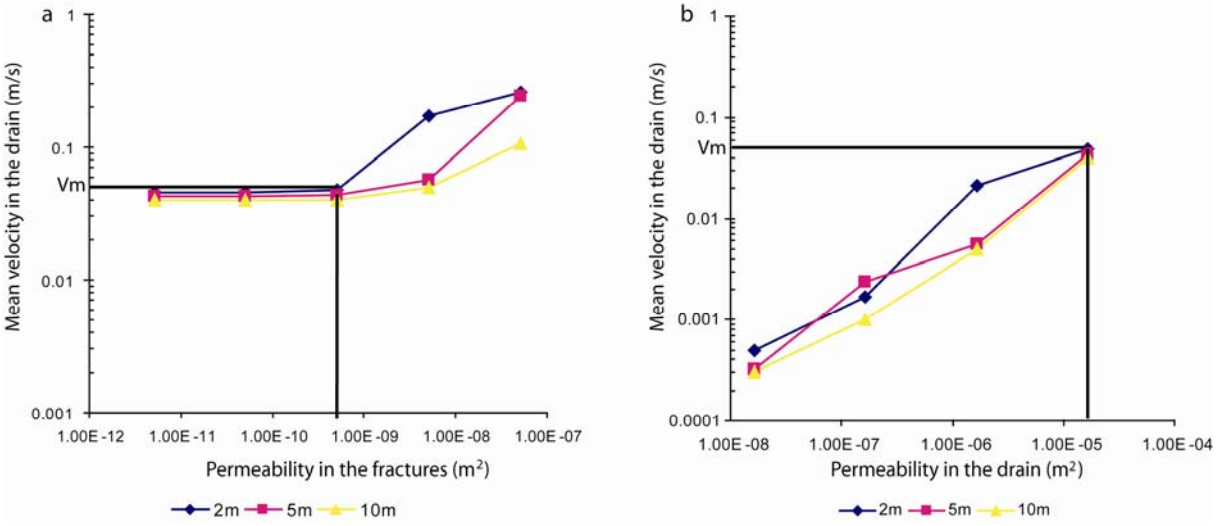
a
b
Mean velocity in the drain (m/s)
Vm
1
0.1
0.01
0.001
0.0001
1.00E-12
1.00E-11
1.00E-10
1.00E-09
1.00E-08
1.00E-07
1.00E-04
1.00E-05
1.00E-06
Permeability in the fractures (m²)
Permeability in the drain (m²)
2m
5m
10m

Figure 4

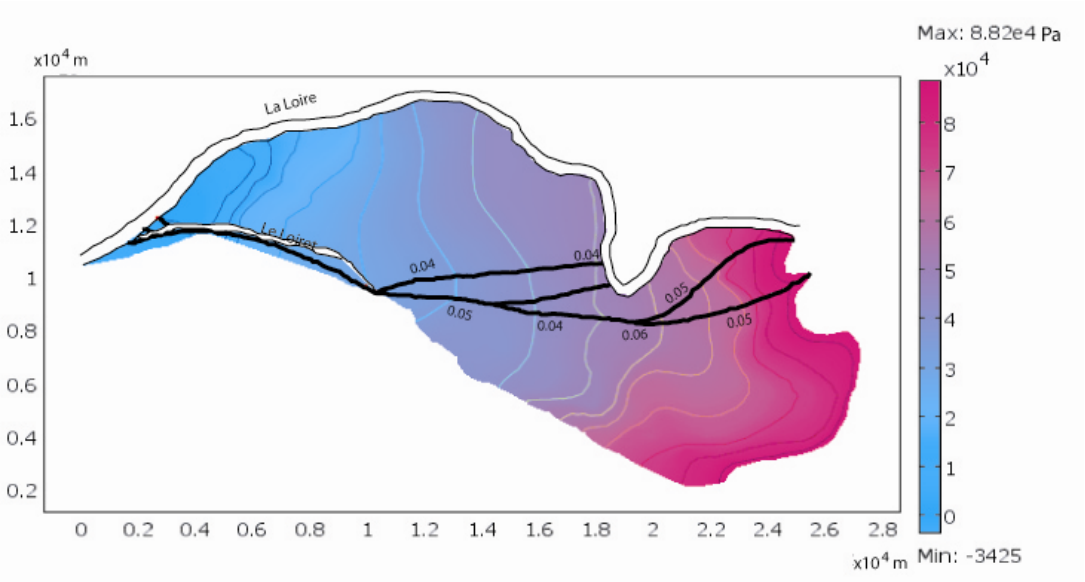
Max: 8.82e4 Pa
x10^4 m
La Loire
Le Loiret
0.04
0.04
0.05
0.05
0.04
0.06
0.05
x10^4
8
7
6
5
4
3
2
1
0
Min: -3425
1.6
1.4
1.2
1
0.8
0.6
0.4
0.2
0
0.2
0.4
0.6
0.8
1
1.2
1.4
1.6
1.8
2
2.2
2.4
2.6
2.8
x10^4 m

Figure 5

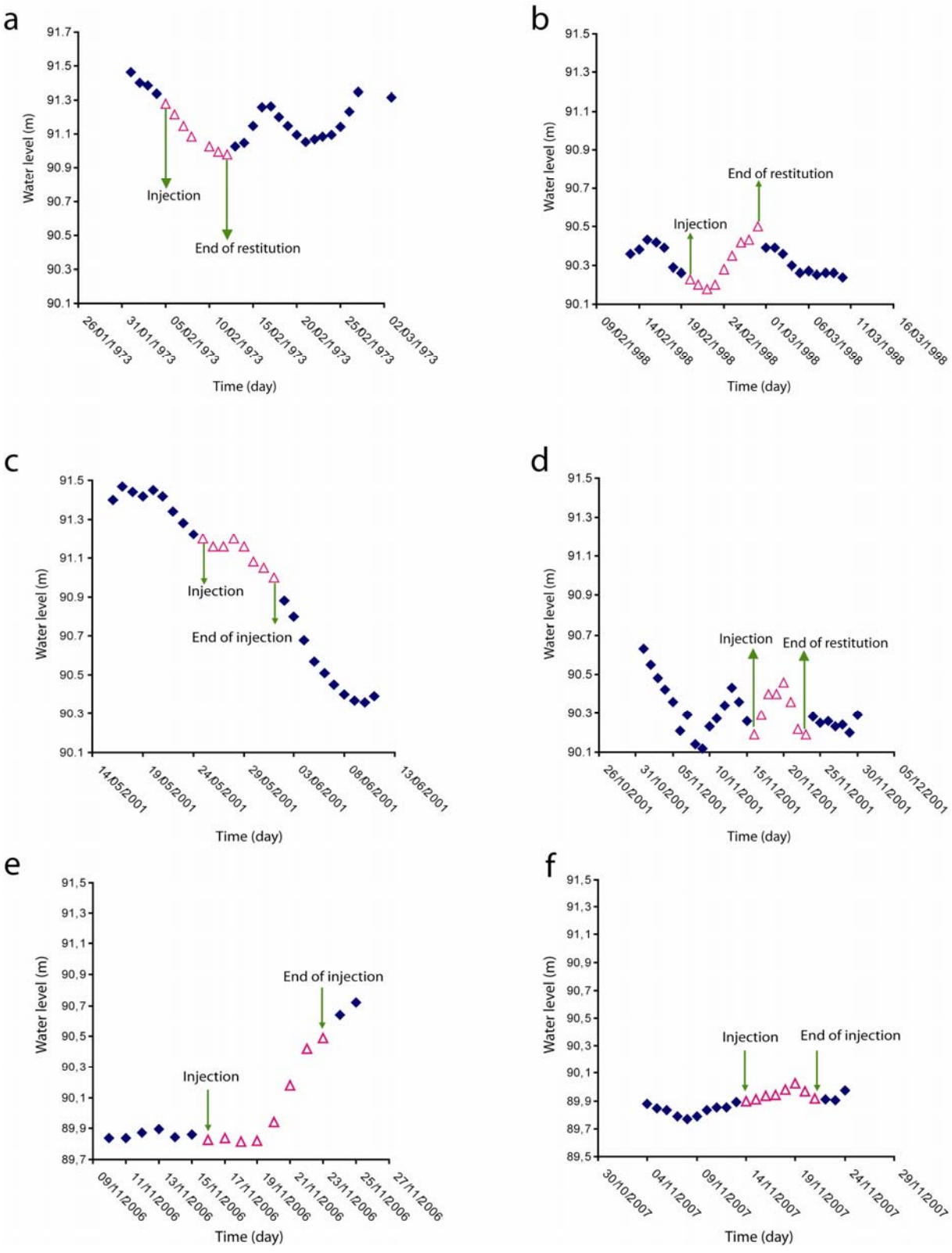
a
Water level (m)
Injection
End of restitution
Time (day)
b
Water level (m)
End of restitution
Injection
Time (day)
c
Water level (m)
Injection
End of injection
Time (day)
d
Water level (m)
Injection
End of restitution
Time (day)
e
Water level (m)
End of injection
Injection
Time (day)
f
Water level (m)
Injection
End of injection
Time (day)

Figure 6

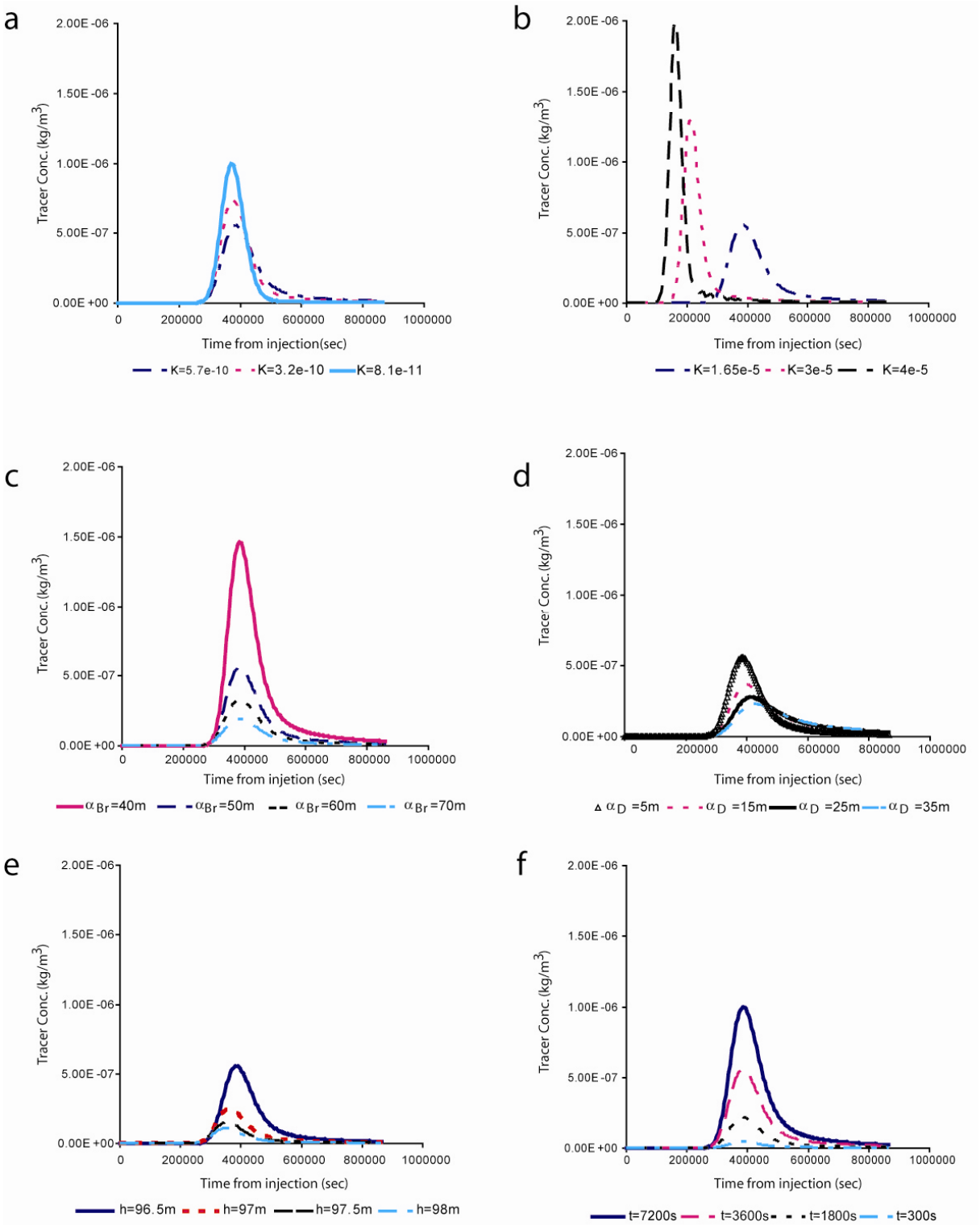
a
2.00E -06
1.50E -06
1.00E -06
5.00E -07
0.00E +00
Tracer Conc. (kg/m3)
0
200000
400000
600000
800000
1000000
Time from injection(sec)
K=5.7e-10
K=3.2e-10
K=8.1e-11
b
Time from injection (sec)
K=1.65e-5
K=3e-5
K=4e-5
c
Time from injetion (sec)
αBr=40m
αBr=50m
αBr=60m
αBr=70m
d
Tracer Conc. (kg/m3)
Time from injection (sec)
αD =5m
αD =15m
αD =25m
αD =35m
e
Time from injection (sec)
h=96.5m
h=97m
h=97.5m
h=98m
f
Time from injection (sec)
t=7200s
t=3600s
t=1800s
t=300s

Figure 7

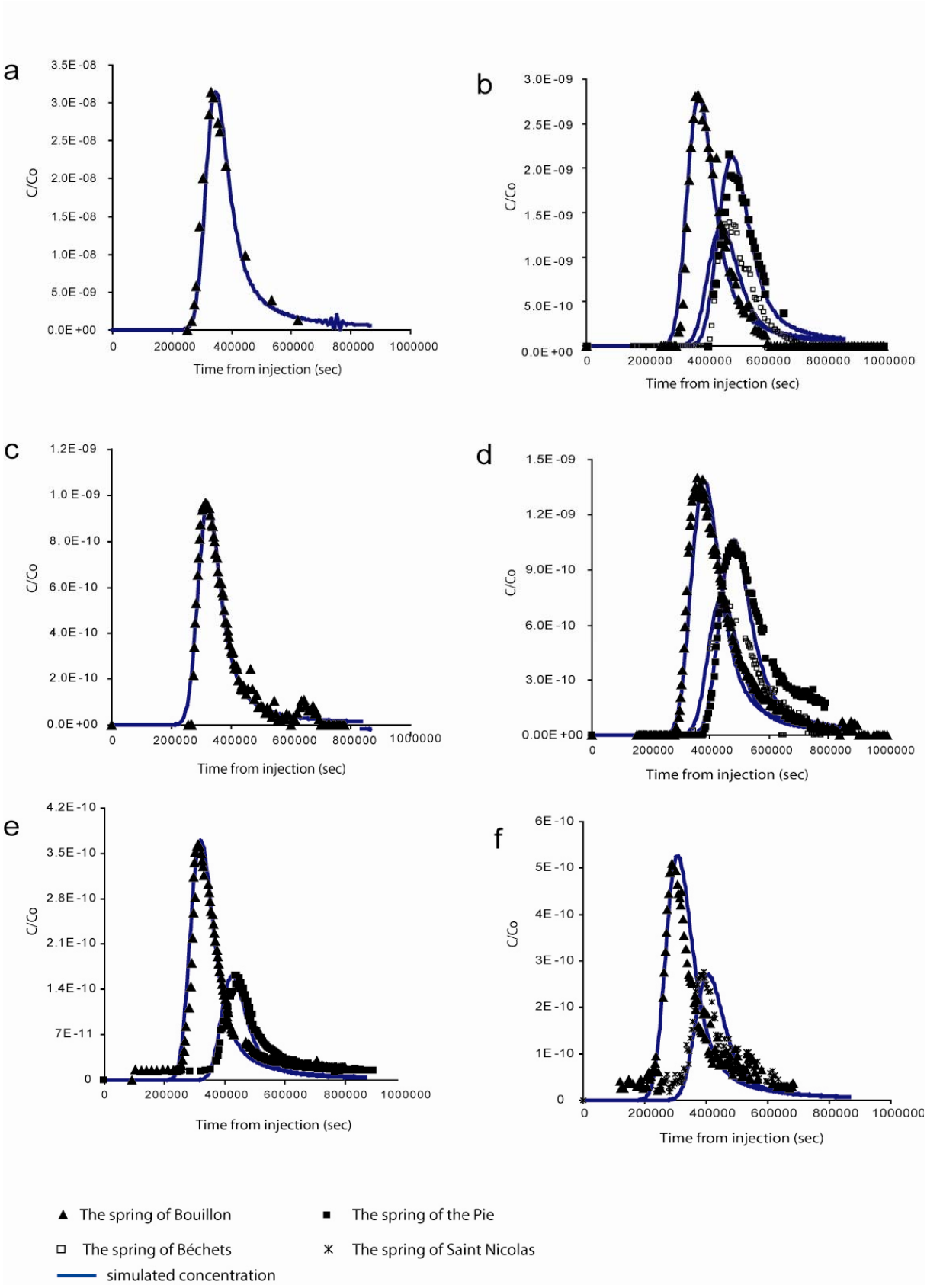
a
3.5E-08
3.0E-08
2.5E-08
2.0E-08
1.5E-08
1.0E-08
5.0E-09
0.0E+00
C/Co
0
200000
400000
600000
800000
1000000
Time from injection (sec)
b
3.0E-09
2.5E-09
2.0E-09
1.5E-09
1.0E-09
5.0E-10
0.0E+00
C/Co
0
200000
400000
600000
800000
1000000
Time from injection (sec)
c
1.2E-09
1.0E-09
8.0E-10
6.0E-10
4.0E-10
2.0E-10
0.0E+00
C/Co
0
200000
400000
600000
800000
1000000
Time from injection (sec)
d
1.5E-09
1.2E-09
9.0E-10
6.0E-10
3.0E-10
0.00E+00
C/Co
0
200000
400000
600000
800000
1000000
Time from injection (sec)
e
4.2E-10
3.5E-10
2.8E-10
2.1E-10
1.4E-10
7E-11
0
C/Co
0
200000
400000
600000
800000
1000000
Time from injection (sec)
f
6E-10
5E-10
4E-10
3E-10
2E-10
1E-10
0
C/Co
0
200000
400000
600000
800000
1000000
Time from injection (sec)
The spring of Bouillon
The spring of the Pie
The spring of Béchets
The spring of Saint Nicolas
simulated concentration

Figure 8

Tracer tests	Samples number				Sampling frequency (hr)	Mass injected (kg)	Spectrofluorimeter limit (ng/ml)
	Spring of Bouillon	Spring of Béchets	Spring of the Pie	Spring of Saint Nicolas			
5 Feb 1973	15	0	0	0	2	15	0.1
20 Feb 1998	100	100	100	0	2	1	0.001
25 may 2001	100	76	0	0	1	2	0.001
15 Nov 2001	200	132	178	0	1	2	0.001
16 Nov 2006	170	0	170	0	1	1	0.0001
14 Nov 2007	190	0	0	106	1	1	0.0001

Table 1

Used curves	calculated parameters
Concentration: C(t)	Time of travel of the leading edge of the tracer cloud : t_1 Time of travel of the trailing edge of the tracer cloud : t_2 Time of the travel of the peak concentration: t_p Duration in time for tracer cloud to pass: $t_d = t_2 - t_1$ Peak concentration of the tracer cloud: Cp Average tracer concentration: $C_{av} = \int_0^{\infty} C(t)dt / t_d$
Flowrate: Q(t)	Volume of flow system traversed before recovery: V_1 $V_1 = \int_0^{t_1} Q(t)dt$ Volume of flow system traversed after recovery: V_2 $V_2 = \int_{t_1}^{t_2} Q(t)dt$
Mass flow: $\varphi(t) = Q(t)C(t)$	Mass of tracer injected: Mo Mass of tracer passing a cross-section: M_r $M_r = \int_0^{\infty} Q(t)C(t)dt$ total tracer recovery (%): $r = M_r / Mo$
Residence time distribution (RTD)	$h(t) = \varphi(t) / M_r = \frac{Q(t)C(t)}{\int_0^{\infty} Q(t)C(t)}$ Mean tracer residence time : $t_m = \int_0^{\infty} th(t)dt$ Variance: $\sigma^2 = \int_0^{\infty} (t - t_m)^2 h(t)dt$

Table 2

Tracer tests	Q mean (l/s)	t_1 (min)	t_2 (min)	t C max (min)	td (min)	C max (ng/ml)	V_1 (m^3)	V_2 (m^3)	% R	MRT (hr)	Variance (min^2)
5 Feb 73	700	4200	10392	5520	6192	5.9	176400	260064	3.7	106	1.4E06
20 Feb 98	300	5029	10047	5989	5018	0.57	90522	90324	2.1	113	9.7E05
25 May 2001	300	4250	11445	5145	7195	0.39	76500	129510	0.7	101	2.1E06
15 Nov 2001	300	4889	14970	6269	10081	0.56	88000	181458	1.4	121	3.5E06
16 Nov 2006	700	4200	11820	5220	7620	0.07	176400	320040	0.66	107	2.8E06
14 Nov 2007	470	3420	11340	4740	7920	0.1	91314	211464	0.65	98	3.3E06

Table 3

Parameters	Recovery time	Varience	R %	MRT
Permeability in the fractured zone (8×10^{-11} - 6×10^{-10} m^2)	No	Strong (291 - 808 hr^2)	Weak (1.36 -1.27)	Strong (107 -120 hr)
Permeability in the drains (1.65×10^{-5} - 5×10^{-5} m^2)	Strong (77 -20hr)	Strong (808 - 514 hr^2)	Strong (1.2 -4.1)	Strong (120 -42 hr)
Dispersivity coefficients in the drains (40 -70 m)	No	Weak (742 - 865 hr^2)	Strong (7.8 -0.5)	No
Dispersivity coefficients in the fractured zone (5-35 m)	Weak (77 -84hr)	Strong (808 -1095 hr^2)	Strong (1.27 -0.85)	Strong (120 -142 hr)
Water level (96.5 -98 m)	Weak (77 -75hr)	No	Strong (1.27 - 4.3)	Strong (120 -111hr)
Injected mass (2 kg -8 kg)	No	No	Strong (1.27- 5.15)	No
α_L / α_T in the drains (1 -0.2)	Strong (77 -142hr)	Strong (808 - 288 hr^2)	Strong (1.2 -54)	Strong (120 -216 hr)
α_L / α_T in the fractured zone (1 -0.2)	No	Weak (808 -515 hr^2)	No	Weak (120 -114 hr)

Table 4

Tracer test		Q mean (l/s)	t_1 (min)	t_2 (min)	t C max (min)	t_d (min)	C max (ng/ml)	$V_1(m^3)$	$V_2(m^3)$	%R	MRT (hr)	Variance (min^2)
6 Feb 73	Measured	700	4200	10392	5520	6192	5.91	176400	260064	3.7	106	1.4E06
	Simulated	914	4200	10920	5760	6720	5.9	230328	368525	4.8	112	3.1E06
20 Feb1998	Measured	300	5029	10047	5989	5018	0.56	90522	90324	2.1	113	9.7E05
	Simulated	350	4080	12780	6109	8700	0.57	85680	182700	2.7	120	2.9E06
25 May 2001	Measured	300	4250	11445	5145	7195	0.39	76500	129510	0.7	101	2.1E06
	Simulated	530	3960	11640	5205	7680	0.39	125928	244224	1.2	104	2.9E06
15 Nov 2001	Measured	300	4889	14970	6269	10081	0.56	88000	181458	1.4	122	3.5E06
	Simulated	314	4680	14400	6480	9720	0.55	88171	183124	1.3	122	3.0E06
16 Nov 2006	Measured	700	4200	11820	5220	7620	0.072	176400	320040	0.66	107	4.9E06
	Simulated	750	3900	11880	5280	7980	0.074	175500	359100	0.68	102	2.9E06
14 Nov 2007	Measured	470	3420	11340	4740	7920	0.001	91314	211464	0.65	98	3.3E06
	Simulated	480	3360	9780	5100	6420	0.001	96768	184896	0.5	87	6.7E05

Table 5